BeBeC-2020-D20

EXPERIMENTAL ASSESSMENT OF IN-DUCT MODAL CONTENT OF FAN BROADBAND NOISE VIA ITERATIVE BAYESIAN INVERSE APPROACH

Antonio Pereira[1] and Marc C. Jacob[1,2]
[1]Univ Lyon, École Centrale de Lyon, INSA Lyon, Université Claude Bernard Lyon I, CNRS,
Laboratoire de Mécanique des Fluides et d'Acoustique, UMR 5509
36, Avenue Guy de Collongue, F-69134 Écully Cedex, France
[2]ISAE-SUPAERO, Département d'Aérodynamique Energétique & Propulsion
10 av. Edouard Belin, B.P. 54032, F-31055 Toulouse Cedex 4, France

Abstract

Next generation of ultra-high-bypass-ratio (UHBR) engines are associated with an increase in fan diameter, a reduction of the exhaust jet speed and shorter intake and exhaust ducts. A direct impact is that the fan module is expected to be the major noise source of commercial aircrafts. It is estimated that the broadband part of fan noise contribution fluctuates about 80-90% in approach conditions and about 40% at take-off. Within this context, an experimental campaign to characterize fan broadband noise has been conducted in the framework of the European project TurboNoiseBB. The experiment has been carried out at the UFFA fan test rig operated by AneCom AeroTest. Different configurations of fan/outlet guide vanes (OGV)-spacing at different working lines have been tested. The radiated noise has been measured by in-duct microphone arrays located at the intake, interstage and downstream of the fan module. A main goal was to assess the modal content of fan broadband noise and further estimate the associated sound power levels. This is done in the present work *via* an iterative Bayesian Inverse Approach (iBIA). One outcome of this approach is an algorithm allowing to control the sparsity degree of the modal content. Thus, different sparsity levels may be tailored to specific noise components (e.g. tonal and broadband contributions) based on *a priori* knowledge. Other advantages are that no assumption regarding inter-modal correlation is necessary and no parameter has to be tuned manually by the end-user.

1. INTRODUCTION

In order to face the steady growth of global air traffic, more and more stringent regulations of noise emissions are imposed. Within an European context, the Advisory Council for Aeronautical Research in Europe (ACARE) has recently confirmed the objective of reducing perceived noise by 65% relative to the year 2000 (Flightpath 2050). At the same time the bypass ratio of turbofan engines has been constantly increasing to cope with the goal of reducing fuel burn consumption. This has lead to the so-called Ultra-High Bypass-Ratio (UHBR) engine architectures. The relative weight of sources contributing to the overall emitted noise has consequently changed and fan noise is currently responsible of 50% to 65% of the aircraft noise at certification points (approach, cutback and sideline). The broadband of that contribution is estimated to fluctuate about 80% to 90% in approach and about 40% at take-off. Thus reducing fan broadband noise has a great potential in reducing aircraft overall noise.

Within this context an extensive experimental campaign aimed at characterizing fan broadband noise and producing reference data for noise predictions has been carried out in the framework of the TurboNoiseBB European Project. Of particular interest in this work are wall-pressure fluctuations data measured through in-duct phased arrays. One of the goals of TurboNoiseBB is the application of advanced techniques for the analysis of the modal content of fan broadband noise. Among these an iterative Bayesian Inverse Approach (iBIA) has been applied. The azimuthal modal content has been assessed both at the intake and the exhaust duct. In addition the noise at the exhaust duct has been decomposed into wavenumber components thanks to a linear phased array. This work has allowed the comparison between the noise generated for two configurations based on different machine geometries. Finally, the estimation of the duct sound power through a complete decomposition (azimuthal and radial) has been compared to estimations based on azimuthal-only and wavenumber decompositions. It is shown that a relatively good agreement is obtained between different estimations.

2. OVERVIEW OF THE EXPERIMENTAL TEST CAMPAIGN

An experimental campaign to characterize fan broadband noise has been carried out in the framework of the TurboNoiseBB project. The experiment has been carried out at the UFFA fan test rig operated by AneCom AeroTest. An extensive database of both acoustic [5, 22] and aerodynamic data [15] has been acquired. A sketch of the ducted test-section in Figure 1(a) depicts the position of mode detection rings relative to the fan. Of particular interest for the present work are the azimuthal ring CMD1 at the intake, as well as the azimuthal ring CMD3 and the axial line array (AX1) both at the bypass section downstream of the Outlet Guide Vanes (OGV).

The tested fan has 20 blades and a diameter of about 34 inches. A set of 44 OGVs is used at two different machine configurations. A first one with a nominal gap between fan and OGVs and a second one with increased fan-OGV distance. The first configuration is called hereafter Short-Gap (SG) and the latter is referred to as Long-Gap (LG). The measurements have been acquired at different rotational speeds for two working lines. The first one being a sea level static working line (SLS-WL) and the second one a low noise working line (LNWL).

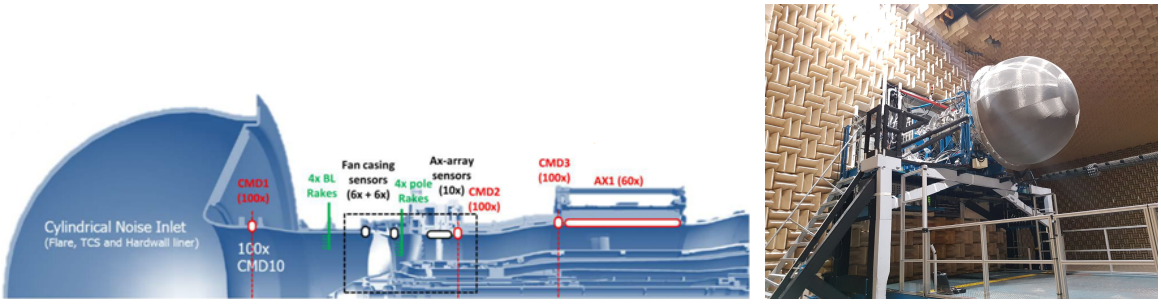

(a) (b)

Figure 1: (a) Sketch of the test-bench showing the different mode detection arrays and (b) a photo showing the intake with the turbulence control screen (TCS) installed.

2.1. Description of the microphone arrays

The test bench has been equipped with various mode detection rings. The goal was to characterize the modal content at the intake, inter-stage and at the by-pass section downstream of OGVs. The intake is equipped with a ring of about 100 kulite® XCS-190 pressure transducers distributed non-uniformly along the duct circumference. This configuration allows to capture the azimuthal modal content up to an azimuthal order of $m = \pm 79$ without aliasing.

The bypass duct is equipped with a combination of a mode detection ring (CMD3) and an axial linear array (AX1). The azimuthal ring is equipped with about 100 Endevco® 8510C piezoresistive pressure transducers. As for the CMD1 array, the probes are non-uniformly distributed along the outer duct casing, allowing a decomposition up to azimuthal order $m = \pm 79$. The axial linear array is composed of 60 G.R.A.S® 40BP pressure microphones. The array axial extent is about $0.8D$ with D the duct diameter and the microphone inter-spacing is of the order of a cm.

3. OUTLINE OF THEORY

This section is organized into three main parts. In the first one a description of the in-duct pressure field using a modal approach is detailed. In the second part, the mode detection problem is formulated using a matrix notation. Finally, the method used to solve the mode detection problem is briefly described.

3.1. Modal description of in-duct pressure field

The acoustic pressure $p(z,r,\phi)$ inside a hard-wall cylindrical duct may be conveniently decomposed as a weighted sum of modes [17]:

$$p(z,r,\phi) = \sum_{m=-\infty}^{\infty} \sum_{n=0}^{\infty} \left[A^{+}_{m,n} \mathrm{e}^{jk^{+}_{m,n}z} + A^{-}_{m,n} \mathrm{e}^{jk^{-}_{m,n}z} \right] f_{m,n}(r) \mathrm{e}^{jm\phi}, \tag{1}$$

with $A^{+}_{m,n}$ and $A^{-}_{m,n}$ the complex-valued coefficients of modes propagating downstream and upstream respectively. The subscripts m and n are the azimuthal and radial mode orders. The terms $k^{\pm}_{m,n}$ are the axial wavenumbers in both downstream $(^{+})$ and upstream $(^{-})$ directions and $f_{m,n}(r)$ is a normalized modal shape factor which depends on the duct's cross section and radial boundary conditions. Expressions for the modal shape factor for both circular and annular duct sections are given in Appendix A. Mode axial wavenumbers $k^{\pm}_{m,n}$ are in turn given by

$$k^{\pm}_{m,n} = -\frac{M_z}{\beta^2} k_0 \pm \hat{k}_{r,m,n}, \tag{2}$$

with $M_z = U_0/c$ the Mach number along the z direction, $\beta^2 = 1 - M_z^2$ the squared Prandtl–Glauert factor and $k_0 = \omega/c$ the acoustic wave number. The term $\hat{k}_{r,m,n}$ is then written

$$\hat{k}_{r,m,n} = \frac{1}{\beta^2}\sqrt{k_0^2 - \beta^2 k_{r,m,n}^2}, \tag{3}$$

where $k_{r,m,n}$ is a radial or transversal wavenumber whose value depends on the boundary conditions at the duct walls, i.e. at $r = r_h$ and $r = r_t$ (see Figure 2). The modeling of the in-duct acoustic pressure through Eq. (1) requires the knowledge of physical quantities such as the mean flow speed and sound speed that in turn depends on the temperature. From an experimental point of view, these values must be accurately measured to ensure an accurate model of the pressure field. Simplifications of Eq. (1) are an interesting approach to avoid this requirement while leading to valuable information. For instance, Eq. (1) may be written as

$$p(\phi) = \sum_{m=-\infty}^{\infty} C_m(z_0, r_0) \mathrm{e}^{jm\phi}, \tag{4}$$

that decomposes a spatial pressure field onto an azimuthal basis with associated azimuthal mode coefficients $C_m(z_0, r_0)$. Notice that these coefficients represent the sum over radial orders n from Eq. (1). Thus, the contribution of both downstream $A^{+}_{m,n}$ and upstream $A^{-}_{m,n}$ modes is intrinsically represented in $C_m(z_0, r_0)$. This is indeed one limitation of this simplification, that is, the contribution of both downstream and upstream propagating modes may not be separated. The dependency of C_m on (z_0, r_0) has been made explicit to emphasize that this decomposition must be carried out at constant axial and radial positions in the duct. For instance, for a ring of acoustic pressure measurements. Another simplification of very practical interest is the decomposition of the in-duct pressure field into its wavenumber components. This can be written as

$$p(z) = \sum_{k_z=-\infty}^{\infty} D_{k_z}(r_0, \phi_0) \mathrm{e}^{jk_z z}, \tag{5}$$

where z is the axial coordinate along the duct axis, r_0 and ϕ_0 are constant radial and azimuthal coordinates and D_{k_z} are the amplitude coefficients of wavenumber components k_z. In practice, due to the limited spatial sampling of linear arrays, aliasing will occur and the maximum wavenumber recovered without ambiguity is $k_{z_{\max}} = \pi/\Delta_z$, Δ_z being the minimum separation distance between microphones. Another limitation concerns the resolution in the wavenumber

domain which is limited by the spatial extent of the array and is given by $\Delta_{k_z} = 2\pi/L_z$, with L_z the array length. Setting the values of wavenumber components k_z from negative to positive values allows to separate waves propagating along both upstream and downstream directions. In addition hydrodynamic components, associated to turbulent boundary layer noise for instance, may also be separated. These are main advantages of this approach. Finally, all presented formulations may be written using a matrix-vector formulation. This is the subject of the next section.

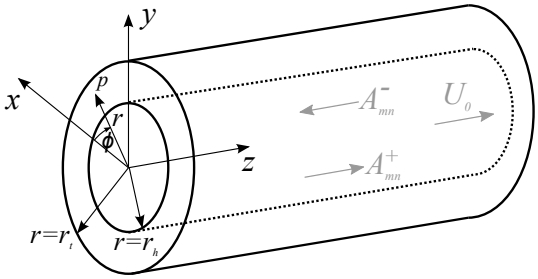

Figure 2: Sketch of the cylindrical coordinates system used in the problem.

3.2. Discussion on the mode detection problem

In order to characterize the in-duct modal content, one approach is to sample the acoustic pressure within the duct and try to estimate the associated complex-valued mode amplitudes. In other words the idea is to discretize the left hand side of Eqs. (1), (4) or (5) and solve for the respective coefficients $A^{\pm}_{m,n}$, C_m and D_{k_z}. For implementation purposes the infinite sums must be truncated, the highest azimuthal order is set to M and highest radial order set to N for instance. A linear system of equations is set between all K measurement positions and all mode coefficients. A matrix-notation version of Eq. (1)is written as

$$\mathbf{p} = \Phi \mathbf{c}, \tag{6}$$

with $\mathbf{p} \in \mathbb{C}^K$ a vector of complex-valued measured pressure at a given frequency ω and $\mathbf{c} \in \mathbb{C}^L$ a vector containing the complex modal coefficients $A^+_{m,n}$ and $A^-_{m,n}$. The dimension L depending on the number of considered azimuthal (M) and radial (N) modes. The matrix $\Phi \in \mathbb{C}^{K\times L}$ is filled with the corresponding terms of the modal basis. The goal is to solve this equation for the mode coefficients $\mathbf{c}$. Whenever the assumption of stationarity and ergodicity of time signals holds, the expression in Eq. (6) may be conveniently written in terms of the cross-spectral matrix of measurements, written by definition as $\mathbf{S_{pp}} \triangleq \mathbb{E}\{\mathbf{p}\mathbf{p}^H\}$. The notation $\cdot^H$ representing the conjugate transpose or the Hermitian of a vector and $\mathbb{E}\{\cdot\}$ to be understood as the expected value over the number of snapshots. Equation (6) then reads

$$\mathbf{S_{pp}} = \Phi \mathbf{S_{cc}} \Phi^H, \tag{7}$$

with $\mathbf{S_{cc}} \triangleq \mathbb{E}\{\mathbf{c}\mathbf{c}^H\}$ the cross-spectral matrix of modal coefficients. The quantity of interest is often the squared value of mode amplitudes, which are simply given by the diagonal terms of $\mathbf{S_{cc}}$. Off-diagonal terms are the cross-spectra between modal coefficients and may be of interest

in cases where mutual coherence between modes is expected, for instance at tonal frequencies. Several techniques and algorithms [12, 14] exist to solve the problem in Eq. 7, either solving for each mode coefficient independently, such as beamforming, or solving the problem as a whole, such as inverse methods.

One typical implementation of beamforming is known as Least-Squares Beamforming [21], the solution for mode coefficients is written as

$$\hat{c}_l = \frac{\boldsymbol{\Phi}_l^H \mathbf{S_{pp}} \boldsymbol{\Phi}_l}{\|\boldsymbol{\Phi}_l\|}, \tag{8}$$

where $\boldsymbol{\Phi}_l$ is the l-th column of matrix Φ and $\hat{c}_l$ is the l-th entry in the diagonal of the cross-spectral matrix of modal coefficients $\hat{\mathbf{S}}_{\mathbf{cc}}$. The off-diagonal terms of $\hat{\mathbf{S}}_{\mathbf{cc}}$ are by definition vanishing, due to the assumption that modal coefficients are mutually incoherent. The advantages of beamforming are its robustness and computational speed. However, a limited resolution and poor quantification results are well-known limitations of beamforming. Inverse methods and deconvolution approaches are alternatives to overcome beamforming limitations at the expense of a higher computational cost. An iterative Bayesian Inverse Approach (iBIA) is applied in the present work. This method has been recently applied to the localization and quantification of aeroacoustic sources, such as jet noise [12] and airframe noise [4, 14]. Theoretical aspects of iBIA are briefly recalled in the next section.

3.3. Overview of the iterative Bayesian Inverse Approach (iBIA)

The idea behind the Bayesian framework applied to inverse problems [2] is to model all unknowns of the problem as random variables. A probabilistic distribution is then assigned to random variables through probability density functions (PDFs). The optimal choice of PDFs will be guided based on *a priori* assumptions and available knowledge of the problem by the user. A significant advantage of the Bayesian approach to ill-posed inverse problems is the generation of tailored regularization techniques [19]. An extensive investigation on different PDFs for the inverse acoustic problem has been recently presented by Antoni et al. [3]. It can be shown that the modeling of unknown variables, in the present work $\mathbf{c}$, by a generalized multivariate complex Gaussian distribution leads to the following minimization problem [11]

$$\hat{\mathbf{c}} = \text{Argmin} \left(\|\mathbf{p} - \Phi\mathbf{c}\|_2^2 + \eta^2 \|\mathbf{c}\|_p^p \right), \tag{9}$$

where by notational convention $\|\mathbf{c}\|_p^p = \sum_{i=1}^N |q_i|^p$ is defined as the ℓ_p-norm of the vector $\mathbf{c}$. The choice of $p = 2$ leads to the classical Tikhonov regularized solution. Other choices of p may be used to control the degree of sparsity of the solution, in particular $p < 2$ is of interest. A study on different choices of p has been done for the problem of noise source localization [11]. No closed-form solution of Eq. (9) exists for values of $p < 2$ since the minimization problem is not quadratic. In this case the Majorization-Minimization (MM) principle [9] may be used to solve it. This leads to an iterative algorithm at which a quadratic function is minimized at each iteration [12, 18]. The resulting algorithm is within the family of Iterative Reweighted Least Squares (IRLS) algorithms [6]. In the following sections a value of $p = 1$ is set for solving the mode detection problem from Eq. (7). Two worth to mention advantages of this approach are: first that no assumption regarding mode inter-correlation is done *a priori* and second that no

further parameters have to be set by the user since the regularization procedure is automated.

4. RESULTS & DISCUSSION

4.1. Single-out fan broadband noise through cyclostationary tools

In order to focus the analysis on fan broadband noise a technique to separate tonal and broadband noise has been applied to the measured data [1]. A tachometer trigger one-pulse per revolution signal has allowed an angular resampling of wall-pressure time signals. This step ensures a regular number of time samples per rotor revolution. Resampled data is then averaged over one or more rotor cycles, depending on the required angular frequency resolution. The deterministic signal obtained in the previous step is then subtracted from raw angular signals. The result is a residual signal whose 1st order cyclo -stationary has been removed. This residual signal contains 2nd and higher order cyclo-stationary components. An example of spectra obtained after this procedure is shown at Fig. 3. Unless otherwise stated, mode detection results shown in upcoming sections have been obtained with data following tone extraction.

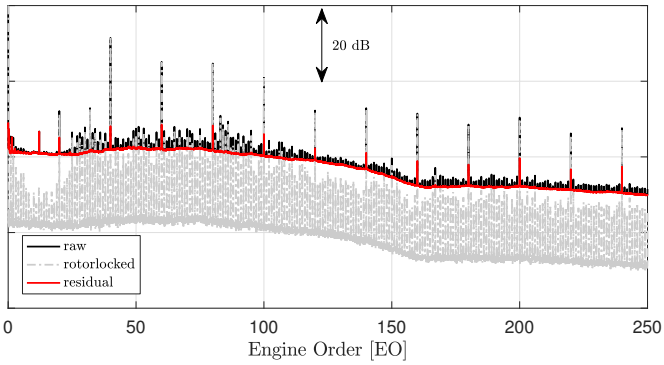

Figure 3: Example of wall-pressure fluctuations spectra measured at the bypass duct mode detection ring (CMD3) that illustrates the separation between tonal and broadband noise. Results show the raw power spectral density (PSD) in black, the rotor-locked tonal noise PSD in gray and the residual spectrum containing the broadband part of measured signals in red. Results are representative of cutback power with a fan speed of 80%ND.

4.2. Intake azimuthal mode plots versus power

The azimuthal modal content at the intake is computed through Eq. (4) with data from microphone ring CMD1, see Figure 1(a). The results are presented as 2D color plots of mode amplitudes versus frequency. Figure 4 shows the results for the short-gap fan-OGV configuration at the sea level static (SLS) working line. The azimuthal modal content is shown as a function of power at the three certification points, namely: approach (50% ND), cutback (80% ND) and sideline (90% ND). Notice that tonal components have been extracted following the procedure from Sec. 4.1.

The structure of mode plots is seen to vary considerably with the increase of fan speed. In particular, a clear change in behavior is observed above 80%, the modal energy tends to be highly concentrated along the cut-on/cut-off boundary. This change in modal structure is more remarkable for the mode plots at the low noise working line (LNWL), see Fig. 5(c). This effect is likely to be related to the generation of shock waves at the rotor blades for transonic/supersonic tip speeds. These shock waves are known to block the passage of downstream generated noise over the fan blades. This might explain the energy reduction at low frequencies observed for the 90% case. At approach power the modal energy is higher at low frequencies up to about 5 kHz. Common to the three tested speeds is a bias towards positive spinning orders m, which are co-rotating modes in the reference frame used here.

An aliasing of co-rotating mode amplitudes onto negative azimuthal orders m is observed at frequencies above 10 kHz. This is related to the azimuthal order limit given by the array geometry, see Sec. 2.1. As the speed increases the occurrence of aliased content is shifted towards lower frequencies.

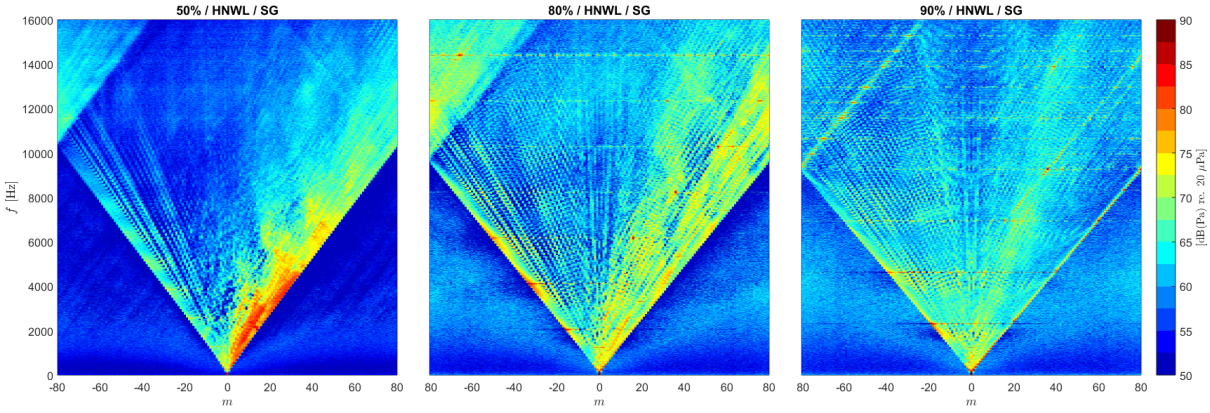

(a) (b) (c)

Figure 4: Azimuthal mode detection plots at the intake as a function of engine power. Results are given for three operating points, namely: (a) approach 50%ND, (b) cutback 80%ND and (c) sideline 90%ND. Results are for the short gap rotor/stator configuration at the sea level static working line (SLS-WL).

In order to quantify the bias towards co-rotating modes for intake mode spectra, the modal amplitudes are integrated over both co-rotating and counter-rotating modes. The resulting spectra are shown at Fig. 6 for approach and cutback power. At lower fan-speeds the gap between co- and counter-rotating modes is significant, see Fig. 6(a). Also noticeable at these spectra are several spectral humps which are not exactly centered at BPF tones. These humps are also present at cutback power, see Fig. 6(b), although they are more spaced apart over frequency and the spectral broadening is wider. Similar behavior of inlet duct wall-pressure spectrum have also been observed elsewhere, see Ref. [8]. It is argued therein that this spectral content might be related to rotor interaction with inlet boundary layer. As the fan speed increases, the level difference between co-rotating and counter-rotating modes is reduced, see Fig. 6(b).

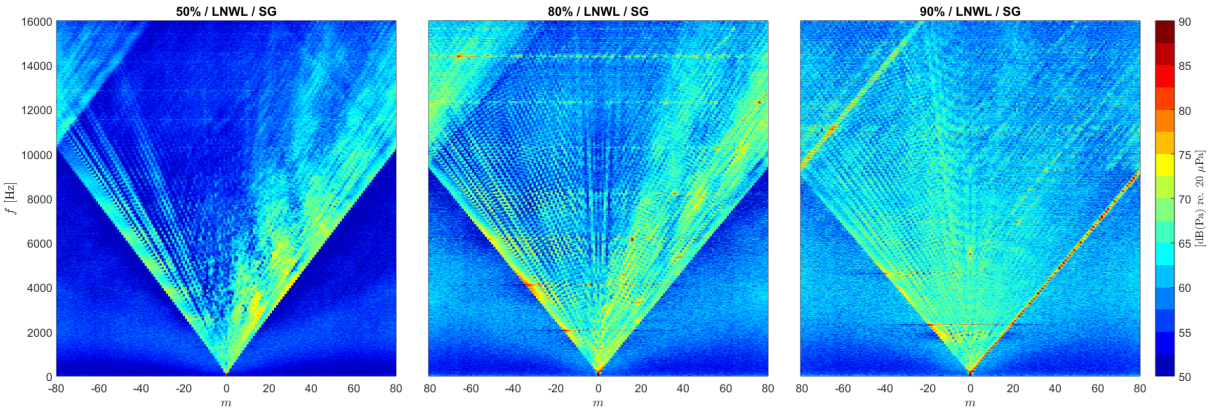

(a) (b) (c)

Figure 5: Azimuthal mode detection plots at the intake as a function of engine power. Results are given for three operating points, namely: (a) approach 50%ND, (b) cutback 80%ND and (c) sideline 90%ND. Results are for the short gap rotor/stator configuration at the low noise working line (LNWL).

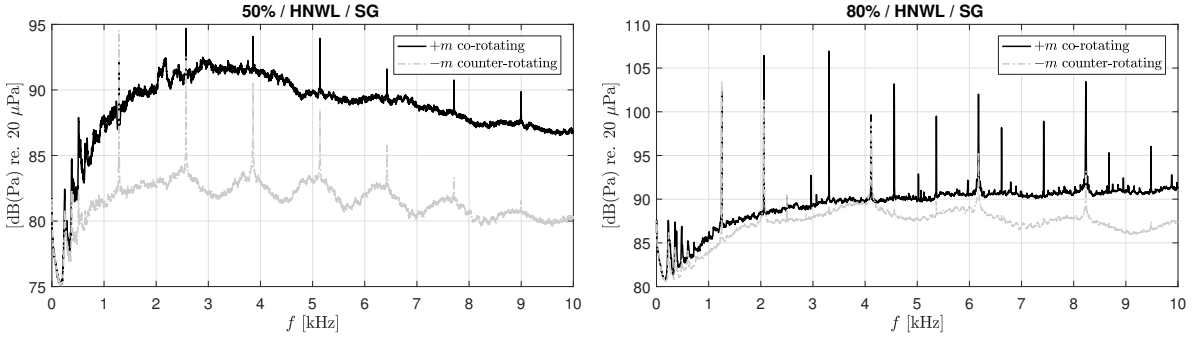

(a) (b)

Figure 6: Integrated intake mode spectra over co-rotating (+m) and counter-rotating (−m) modes for two fan speeds: (a) approach 50%ND and (b) cutback 80%ND. The results are given for the short fan-OGV gap at the sea level static working line (SLS-WL).

4.3. Bypass-duct azimuthal mode plots versus power

The azimuthal mode content at the bypass duct downstream of OGVs is shown in Fig. 7 for increasing engine power. The results are obtained using the data from the downstream mode detection ring CMD3, see Fig. 1(a). It can be noticed that contrary to intake mode plots no clear bias towards co- or counter-rotating modes exists. A slight bias towards counter-rotating modes is noticeable for modes well above cut-on, however. As frequency increases the energy of mode plots tends to be rather concentrated on modes well above cut-on, with lower azimuthal orders. The general modal structure does not change drastically with increasing power, as compared to intake mode plots. However, the modal energy is seen to gradually increase from lower (see approach) to higher speeds (cutback and sideline). The effect of aliasing is not clearly seen as

compared to intake mode plots. This is because pressure levels are much lower for modes close to the cuton/cutoff boundary.

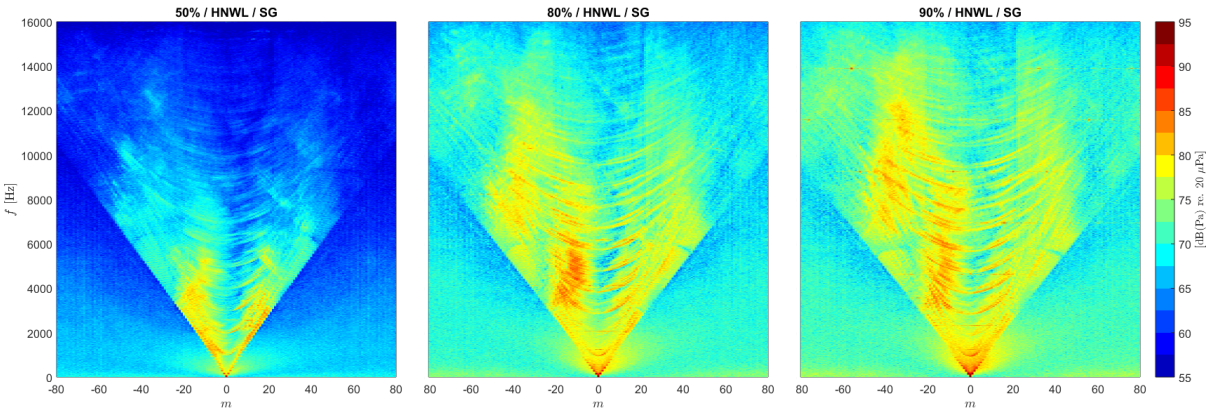

(a) (b) (c)

Figure 7: Azimuthal mode detection plots at the bypass duct as a function of engine power. Results are given for three operating points, namely: (a) approach 50%ND, (b) cutback 80%ND and (c) sideline 90%ND. Results are for the short gap rotor/stator configuration at the sea level static working line (SLS-WL).

The azimuthal mode detection maps have been integrated over both co-rotating and counter-rotating modes. Resulting spectra are shown in Fig. 8 at approach and sideline power. Compared to intake mode spectra, see Fig. 6, the levels are more evenly balanced between co-rotating and counter-rotating modes. As frequency increases, however, a bias towards counter-rotating modes is observed for both approach and sideline power. The level difference is of the order of 3 dB.

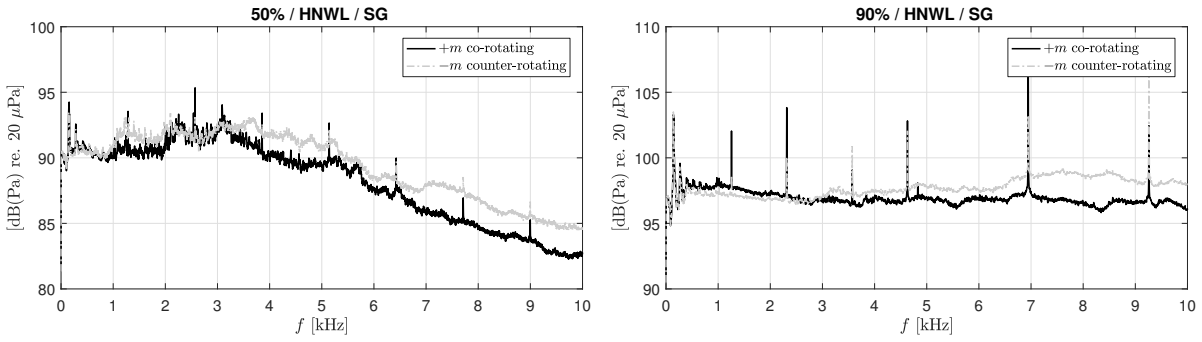

(a) (b)

Figure 8: Integrated bypass mode spectra over co-rotating (+m) and counter-rotating (−m) modes for two fan speeds: (a) approach 50%ND and (b) sideline 90%ND. The results are given for the short fan-OGV gap at the sea level static working line (SLS-WL).

4.4. Wavenumber decomposition at the bypass-duct

The test bench is equipped with a linear microphone array at the bypass-duct downstream of OGVs, as outlined in Sec. 2.1. Several post processing techniques may be applied using this kind of array geometry, in duct beamforming [13, 24] and wavenumber decompositions are common examples [7, 20, 22]. In the present work a wavenumber decomposition is performed through the formulation given by Eq. (5). Figure 9 shows the wavenumber domain spectra at different fan speeds, namely: approach, cutback and sideline. Few remarks are of importance for the interpretation of results. First, aliased wavenumber components are clearly seen on the 2D color plots. These are due to the limited inter-microphone axial separation distance, which is of the order of a cm. Two types of aliased data are apparent. The first one is related to the hydrodynamic-associated component with a slope dependent on the velocity at which turbulent structures are convected downstream. The aliased data appear at the negative wavenumber domain at frequencies around 3 to 5 kHz, depending on the fan speed. When aliased data overlaps the acoustic domain, care should be taken to interpret results. A second type is related to the aliasing of upstream acoustic components (negative wavenumbers) into the positive wavenumber domain. This contribution arises at higher frequencies, tipycally above 10 kHz. A clear separation between acoustic and hydrodynamic components is obtained, except at very low frequencies. Notice the inclination of the "V-shaped" acoustic domain in the anti-clockwise direction due to the convective effect of the mean flow. The inclination increases with increasing fan speed. The structure of wavenumber decomposition plots is rather similar for all tested fan speeds, with most energy concentrated on positive wavenumber domain, that is, sound propagating downstream in the duct. The "U-shaped" structures apparent at the acoustic domain data are related to the axial wavenumber of duct modes, see Eq. (2).

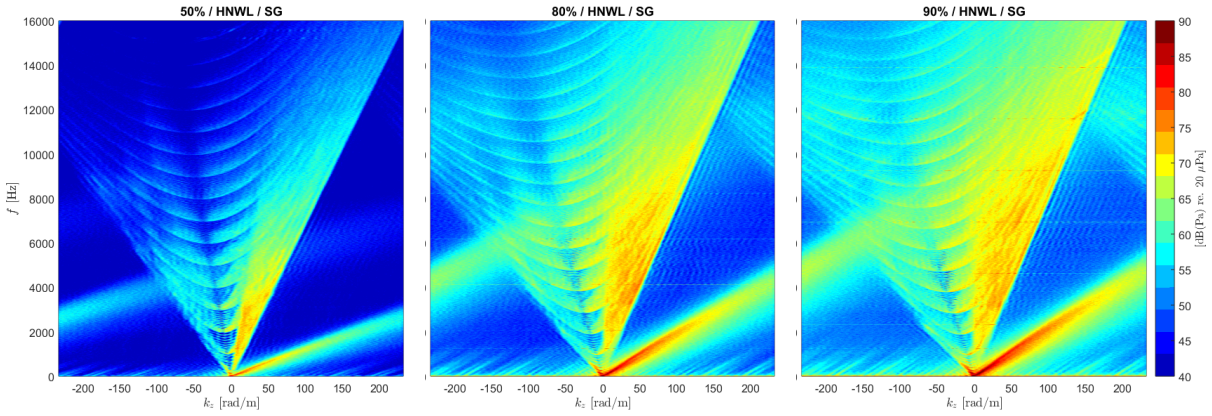

(a) (b) (c)

Figure 9: Wavenumber decomposition plots obtained at the bypass-duct as a function of engine power. Results are given for three operating points, namely: (a) approach 50%ND, (b) cutback 80%ND and (c) sideline 90%ND. Results are for the short gap rotor/stator configuration at the sea level static working line (SLS-WL).

4.5. Influence of the fan/OGV separation distance

As mentioned in Sec. 2 two different fan-OGV inter-spacings have been tested during the TNBB experimental campaign. In this section, a comparison is made between both configurations using in-duct wall-pressure fluctuations data. In particular, the modal content estimated through the different microphone arrays will be used for the analysis. The influence on the noise measured at both intake and bypass-duct is assessed.

Noise measured at the intake duct

Azimuthal mode detection plots for both the short-gap (SG) and long-gap (LG) OGV configurations are shown in Fig. 10. The structure of mode plots do not change considerably when comparing LG and SG configurations at the fan speeds of 50%ND and 60%ND. Although levels for positive spinning modes are slightly higher for the SG. Looking at mode plots estimated at 100%ND, see Figs. 10(c) and 10(f), a significant level increase on positive spinning modes close to cut-off is noticed for the SG configuration.

In order to ease the comparison, mode pressure levels are integrated over both co-rotating and counter-rotating mode amplitudes as done in previous sections. Integrated mode spectra at approach power are shown in Fig. 11(a). As can be seen, the conclusions differ for co-rotating or counter-rotating mode spectra. For the first, pressure levels for both SG and LG are equivalent from low frequencies up to 2 kHz. As frequency increases, the LG configuration shows pressure levels at the order of 3dB lower than the SG configuration. For the counter-rotating pressure spectra, no difference is observed between SG and LG configurations over the whole frequency band. This result suggests that the source mechanism at the origin of this counter-rotating intake noise is not altered by the presence of the stator behind the rotor, that would be the case of rotor interaction with inlet boundary layer. On the other hand, co-rotating mode spectra suggests that the source mechanism is an interaction between fan and OGV. The results at 60%ND fan speed indicate that the noise reduction of LG configuration reduces as the fan speed increases. One possible explanation is that the balance between different noise sources is changed with increasing speed.

Noise measured at the bypass-duct

The influence of fan-OGV separation distance on the noise at the bypass-duct is assessed in Fig. 12 for the approach condition. The trends are quite similar for both co-rotating and counter-rotating mode spectra. The long-gap OGV configuration leads to relatively higher levels at lower frequencies and a reduction of noise at higher frequencies. The noise reduction seems to be more important for counter-rotating modes, see Fig. 12(b). This observation is in agreement with the argument that a larger separation allows a reduction of turbulent wake intensity, a widening of wakes and an increase of turbulence length scales. The intensity reduction would lead to a decrease of noise levels. The increase of length scales would lead to an increase of levels at low frequencies and a reduction at high frequencies.

Different observations are found for increasing fan rotational speeds, as seen in Fig. 13 at sideline power. In this case the frequency band at which levels are increased for LG configuration are even wider, up to about 8 kHz.

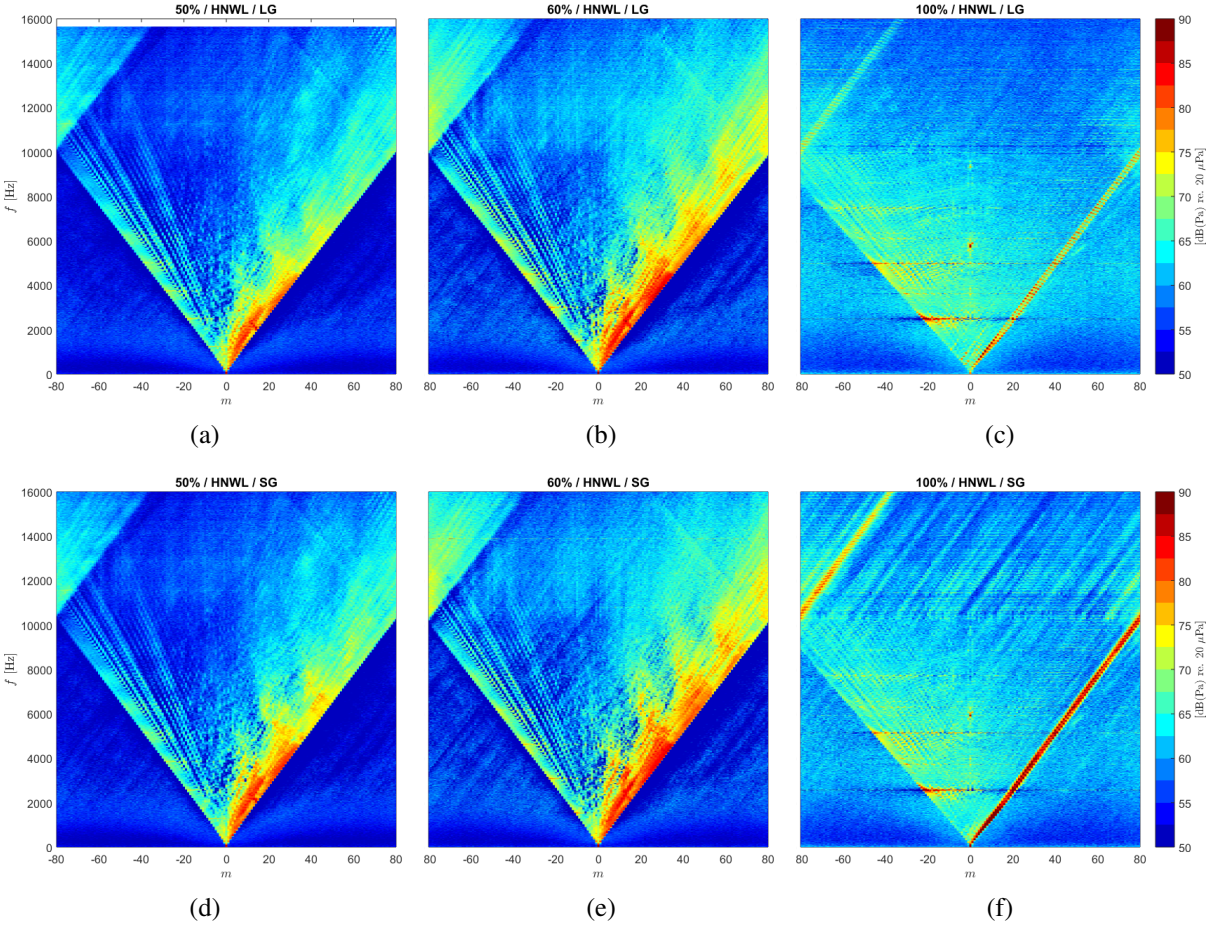

Figure 10: Influence of the fan-OGV separation distance on the azimuthal mode content estimated at the intake duct. Top row: ***long-gap OGV*** *results; Bottom row:* ***short-gap OGV*** *results. Mode plots are shown for the following three fan speeds at the SLS-WL: (a,d) 50%ND; (b,e) 60%ND and (c,f) 100%ND.*

4.6. Estimation of the duct sound power

The decomposition of in-duct pressure field into azimuthal and radial modes, see Eq. (1), allows for a direct computation of the duct sound power [16]. The relation between mode acoustic power and modal amplitudes are given by the following equation:

$$W_{mn}^{\pm} = \frac{\pi k_0 \beta^4}{Z_0} \frac{\hat{k}_{r,m,n}}{\left(k_0 \mp M_z \hat{k}_{r,m,n}\right)} \left|A_{m,n}^{\pm}\right|^2, \tag{10}$$

with $Z_0 = \rho_0 c$ the acoustic impedance and $\hat{k}_{r,m,n}$ as given by Eq. (3). Equation (10) gives the sound power carried by each individual mode W_{mn}. The total transmitted sound power along the duct is often of interest. The integration of Eq. (10) over azimuthal and radial mode orders

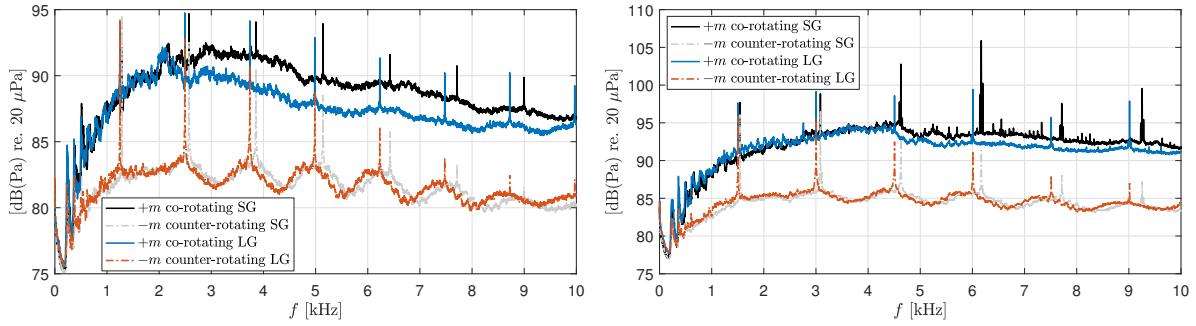

(a) (b)

Figure 11: Intake mode spectra integrated over co-rotating (+m) and counter-rotating (−m) modes both the short-gap and long-gap OGV configurations. Results are shown for two fan speeds: (a) 50%ND and (b) 60%ND.

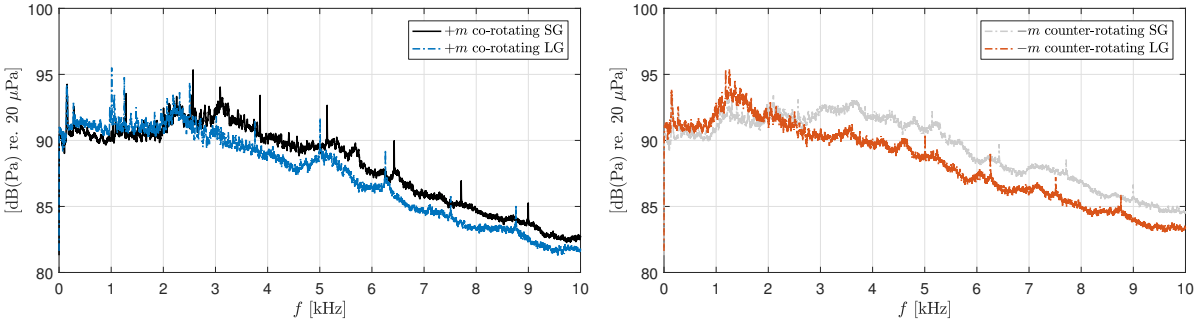

(a) (b)

Figure 12: Influence of the fan-OGV separation distance on the noise measured at the bypass-duct at approach power. Figure shows integrated mode amplitudes for SG and LG configurations for: (a) co-rotating modes and (b) counter-rotating modes.

gives the total in-duct sound power transmitted either downstream W^+ or upstream W^-:

$$W^{\pm} = \frac{\pi k_0 \beta^4}{Z_0} \sum_{m=-M}^{M} \sum_{n=0}^{N} \frac{\hat{k}_{r,m,n}}{\left(k_0 \mp M_z \hat{k}_{r,m,n}\right)} \left|A^{\pm}_{m,n}\right|^2, \tag{11}$$

where M and N are respectively the maximum azimuthal and radial orders considering only cut-on modes. Often it is not possible to obtain a complete modal breakdown since it requires a relatively large number of microphones distributed over azimuthal and axial positions. It is of interest thus to obtain an estimate of in-duct sound power based on azimuthal-only or wavenumber decompositions. Although this requires an assumption regarding the distribution of the modal energy. This has been investigated by Joseph et al. [10], where different assumptions on the modal distribution have been studied. An assumption which is commonly adopted for fan broadband noise is the Equal Energy Density per Mode (EEDM). This is the assumption tested here for the computation of duct sound power based on both azimuthal-only and wavenum-

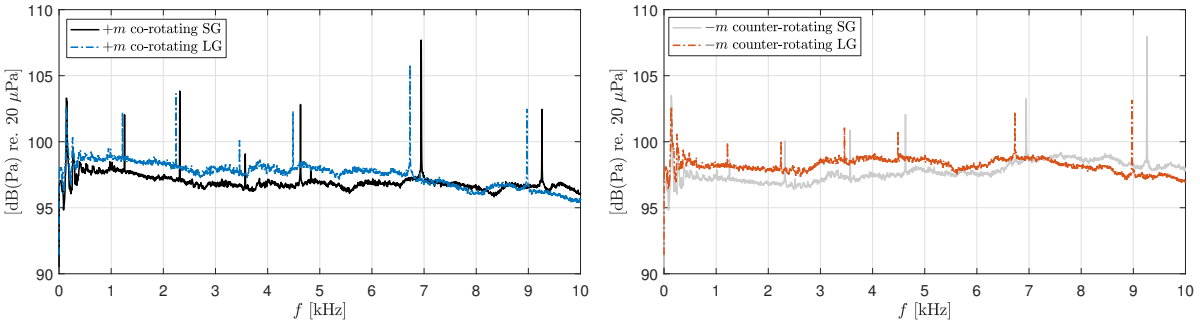

(a) (b)

Figure 13: Influence of the fan-OGV separation distance on the noise measured at the bypass-duct at sideline power. Figure shows integrated mode amplitudes for SG and LG configurations for: (a) co-rotating modes and (b) counter-rotating modes.

ber decompositions. These estimations are then compared to sound power computed directly through Eq. (11). Results of the comparison are shown in Fig. 14 for two operating points representative of approach and cutback power. The different estimations agree relatively well over the whole frequency band. The sound power estimated from azimuthal-only decomposition at low frequencies are several dB's higher than the others. This trend is seen to increase with increasing fan speed. This result is somewhat expected since azimuthal-only decomposition (AMD) does not allow the separation between downstream and upstream propagating modes. This would lead to an overestimation of levels. In addition, the results from both AMD and ARMD (azimuthal and radial modal decomposition) may be corrupted by hydrodynamic-associated noise at low frequencies. On the other hand, the wavenumber decomposition (WND) allows to filter-out this contribution.

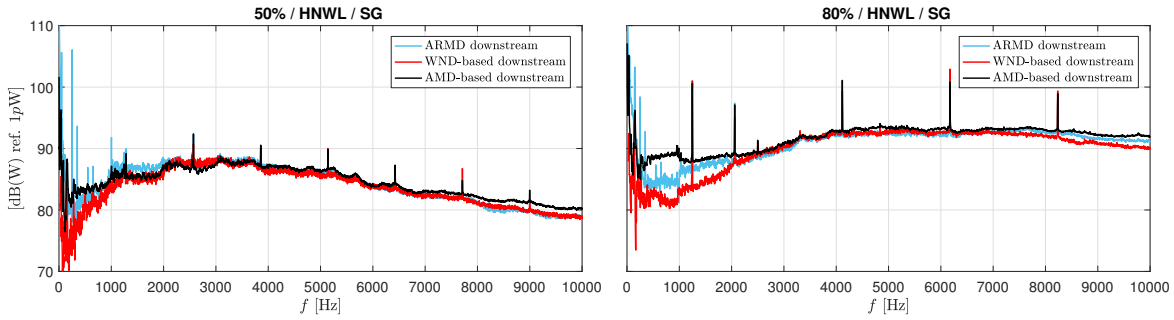

(a) (b)

Figure 14: Comparison between different estimations of the in-duct sound power at the bypass-duct. ARMD: Azimuthal and Radial Modal Decomposition, WND: Wavenumber Decomposition-based and AMD: Azimuthal Modal Decomposition-based. Results are given for the sea level static working line and for the short-gap OGV configuration at (a) approach 50%ND and (b) cutback 80%ND.

5. CONCLUSIONS

Fan broadband noise is responsible for a major part of aircraft overall noise for future UHBR engine architectures. To improve understanding of its generation mechanisms an extensive experimental database has been acquired within the TurboNoiseBB project. The present work has been focused in the analysis of broadband noise at both the intake duct and the bypass section of a rotor/stator stage.

Azimuthal mode detection and wavenumber decomposition of wall-pressure fluctuations data have been computed. The application of an iterative Bayesian Inverse Approach (iBIA) has allowed results with improved dynamic range and limited aliasing by the introduction of sparsity enforcing constraints.

A short-gap and a long-gap OGV configuration have been compared in terms of the noise generated both at the intake and the bypass duct. Increasing the rotor-stator spacing has shown reduced levels at higher frequencies for intermediate fan speeds (see approach) for both inlet and exhaust noise. With increasing fan speed the difference between SG and LG configurations tends to decrease and LG even showing higher levels for exhaust noise at low frequencies. Although, it is important to mention that the fan was not designed to work on a LG build and the same OGV set has been used for both configurations. In addition a modification of the duct casing has been done for the LG mounting.

The in-duct sound power has been estimated through three different approaches. One based in a complete modal breakdown and other two requiring an assumption on the modal distribution. A good agreement between these approaches has been found mainly at medium to high frequencies using a Equal Energy Density per Mode distribution. The agreement at low frequencies is hindered by the presence of strong hydrodynamic disturbances due to the flow and the impossibility to separate downstream and upstream modes for the azimuthal-only decomposition. These results supports the assumption of EEDM distribution commonly used for fan broadband noise.

Acknowledgements

The presented work was conducted in the frame of the project TurboNoiseBB, which has received funding from the European Union's Horizon 2020 research and innovation program under grant agreement No. 690714. It was also performed within the framework of the Labex CeLyA of the Université de Lyon, within the program "Investissements d'Avenir" (ANR-10-LABX-0060/ANR-16-IDEX-0005) operated by the French National Research Agency (ANR).

The authors kindly acknowledge all the team from TurboNoiseBB involved in the test campaign.

A. Normalized mode shape factors

A.1. Circular cross section

The normalized modal shape factor for a circular duct (see Ref. [23]) may be written as:

$$f_{m,n}(r) = \frac{J_{|m|}(k_{r,m,n}r)}{\Gamma_{m,n}}, \tag{12}$$

with $k_{r,m,n}$ a radial or transversal wavenumber whose value depends on the boundary condition at the duct wall, $J_{|m|}(\cdot)$ is the m-th order Bessel function and $\Gamma_{m,n}$ is a normalization factor introduced to ensure that the modal shape functions are orthonormal, that is, orthogonal and normalized over the duct's cross section.

A.2. Annular cross section

The radial shape factors for an annular duct may be expressed as

$$f_{m,n}(r) = \frac{1}{\Gamma_{m,n}}\left(J_{|m|}(k_{r,m,n}r) + CY_{|m|}(k_{r,m,n}r)\right), \tag{13}$$

with $J_{|m|}(\cdot)$ and $Y_{|m|}(\cdot)$ the m-th order Bessel and Neumann functions respectively and the coefficient C is given by

$$C = -\frac{J'_{|m|}(k_{r,m,n}r_t)}{Y'_{|m|}(k_{r,m,n}r_t)}, \tag{14}$$

with $J'_{|m|}(\cdot)$ and $Y'_{|m|}(\cdot)$ the first derivatives of Bessel and Neumann functions and r_t the radius at the outer duct casing.

References

[1] J. Antoni. "Cyclostationarity by examples." *Mechanical Systems and Signal Processing*, 23(4), 987 – 1036, 2009.

[2] J. Antoni. "A bayesian approach to sound source reconstruction: Optimal basis, regularization, and focusing." *The Journal of the Acoustical Society of America*, 131(4), 2873–2890, 2012.

[3] J. Antoni, T. L. Magueresse, Q. Leclère, and P. Simard. "Sparse acoustical holography from iterated bayesian focusing." *Journal of Sound and Vibration*, 446, 289–325, 2019.

[4] C. J. Bahr, W. M. Humphreys, D. Ernst, T. Ahlefeldt, C. Spehr, A. Pereira, Q. Leclère, C. Picard, R. Porteous, D. Moreau, J. R. Fischer, and C. J. Doolan. "A comparison of microphone phased array methods applied to the study of airframe noise in wind tunnel testing." In *23rd AIAA/CEAS Aeroacoustics Conference*. American Institute of Aeronautics and Astronautics, 2017.

[5] M. Behn and U. Tapken. "Investigation of sound generation and transmission effects through the ACAT1 fan stage using compressed sensing-based mode analysis." In *25th AIAA/CEAS Aeroacoustics Conference*. American Institute of Aeronautics and Astronautics, 2019.

[6] I. Daubechies, R. DeVore, M. Fornasier, and C. S. Güntürk. "Iteratively reweighted least squares minimization for sparse recovery." *Communications on Pure and Applied Mathematics*, 63(1), 1–38, 2010.

[7] R. P. Dougherty and R. Bozak. "Two-dimensional modal beamforming in wavenumber space for duct acoustics." In *2018 AIAA/CEAS Aeroacoustics Conference*. American Institute of Aeronautics and Astronautics, 2018.

[8] U. W. Ganz, P. D. Joppa, T. J. Patten, and D. F. Scharpf. "Boeing 18-inch fan rig broadband noise test." Technical Report CR-1998-208704, NASA, 1998.

[9] D. R. Hunter and K. Lange. "A tutorial on mm algorithms." *The American Statistician*, 58(1), 30–37, 2004.

[10] P. Joseph, C. Morfey, and C. Lowis. "Multi-mode sound transmission in ducts with flow." *Journal of Sound and Vibration*, 264(3), 523–544, 2003.

[11] Q. Leclère, A. Pereira, and J. Antoni. "Une approche bayésienne de la parcimonie pour l'identification de sources acoustiques." In *12ème Congrès Français d'Acoustique, Poitiers, France*. 2014.

[12] Q. Leclère, A. Pereira, C. Bailly, J. Antoni, and C. Picard. "A unified formalism for acoustic imaging based on microphone array measurements." *International Journal of Aeroacoustics*, 16(4-5), 431–456, 2017.

[13] C. Lowis, P. Joseph, and A. Kempton. "Estimation of the far-field directivity of broadband aeroengine fan noise using an in-duct axial microphone array." *Journal of Sound and Vibration*, 329(19), 3940 – 3957, 2010.

[14] R. Merino-Martínez, P. Sijtsma, M. Snellen, T. Ahlefeldt, J. Antoni, C. J. Bahr, D. Blacodon, D. Ernst, A. Finez, S. Funke, T. F. Geyer, S. Haxter, G. Herold, X. Huang, W. M. Humphreys, Q. Leclère, A. Malgoezar, U. Michel, T. Padois, A. Pereira, C. Picard, E. Sarradj, H. Siller, D. G. Simons, and C. Spehr. "A review of acoustic imaging methods using phased microphone arrays." *CEAS Aeronautical Journal*, 10(1), 197–230, 2019.

[15] R. Meyer, S. Hakanson, W. Hage, and L. Enghardt. "Instantaneous flow field measurements in the interstage section between a fan and the outlet guiding vanes at different axial positions." In *ETC13, Lausanne, Switzerland*. 2019.

[16] C. Morfey. "Sound transmission and generation in ducts with flow." *Journal of Sound and Vibration*, 14(1), 37–55, 1971.

[17] M. Munjal. *Acoustics of ducts and mufflers with application to exhaust and ventilation system design*. Wiley, 1987.

[18] A. Pereira. *Acoustic imaging in enclosed spaces*. Ph.D. thesis, INSA de Lyon, 2013.

[19] A. Pereira, J. Antoni, and Q. Leclère. "Empirical bayesian regularization of the inverse acoustic problem." *Applied Acoustics*, 97, 11 – 29, 2015.

[20] E. Salze, E. Jondeau, A. Pereira, S. L. Prigent, and C. Bailly. "A new MEMS microphone array for the wavenumber analysis of wall-pressure fluctuations: application to the modal investigation of a ducted low-mach number stage." In *25th AIAA/CEAS Aeroacoustics Conference*. American Institute of Aeronautics and Astronautics, 2019.

[21] P. Sijtsma. "Experimental techniques for identification and characterisation of noise sources,." In *Advances in Aeroacoustics and Applications*. VKI Lecture Series, 5:15–19, 2004.

[22] U. Tapken, M. Behn, M. Spitalny, and B. Pardowitz. "Radial mode breakdown of the ACAT1 fan broadband noise generation in the bypass duct using a sparse sensor array." In *25th AIAA/CEAS Aeroacoustics Conference*. American Institute of Aeronautics and Astronautics, 2019.

[23] U. Tapken and L. Enghardt. "Optimization of sensor arrays for radial mode analysis in flow ducts." In *Proceedings of the 12th AIAA/CEAS Aeroacoustics Conference, Cambridge, Massachusetts, USA*, 2638. 2006.

[24] B. J. Tester and Y. Özyörük. "Predicting far-field broadband noise levels from in-duct phased array measurements." In *20th AIAA/CEAS Aeroacoustics Conference*. American Institute of Aeronautics and Astronautics, 2014.